Rheol Acta (2002) 41: 45–54

ORIGINAL CONTRIBUTION

Gudrun Schmidt
Alan I. Nakatani
Charles C. Han

Rheology and flow-birefringence from viscoelastic polymer-clay solutions

Received: 25 January 2001
Accepted: 22 May 2001

G. Schmidt (✉) · A. I. Nakatani
C. C. Han
Polymers Division
National Institute of Standards
and Technology, Gaithersburg
Maryland 20899, USA
e-mail: Gudrun.Schmidt@chem.lsu.edu

Certain equipment and instruments or materials are identified in this paper in order to specify adequately the experimental details. Such identification does not imply recommendation by the National Institute of Standards and Technology nor does it imply the materials are the best available for the purpose.

Abstract The shear orientation of viscoelastic clay-polymer solutions was investigated by means of rheology and flow birefringence (Δn). The polymer chains are in dynamic adsorption/desorption equilibrium with the clay particles to form a "network". The elastic behavior of the network was characterized by constant stress, oscillatory shear, and stress relaxation experiments. Constant stress experiments indicated a yield stress upon which shear flow started and no strain recovery could be observed. Oscillatory shear experiments showed a broad elastic region followed by flow when a critical strain was reached. Stress relaxation experiments showed several relaxation times when the same critical strain was reached. Experiments under steady flow characterized the transient behavior of the network. With increasing steady shear rate a pronounced minimum in birefringence was observed at a critical shear rate. The shear rate dependent viscosity showed near power law behavior and no corresponding critical feature. While birefringence detects orientational effects on a microscopic length scale, rheology averages over macroscopic changes in the sample. The same degree of orientation could be achieved under constant shear rate or constant stress conditions.

Key words Clay · Polymer · Flow-birefringence · Network · Solution

Introduction

Shear-induced structural changes in complex fluids of anisotropic species are a very general problem encountered not only in polymer solutions (Nakatani and Dadmun 1995; Sondergaard and Lyngaae-Jorgensen 1995) but also in liquid crystalline materials (Jamieson et al. 1996; Roux et al. 1993; Schmidt et al. 1998), block copolymer melts (Bates et al. 1994; Nakatani and Dadmun 1995; Nakatani et al. 1996), and in plate-like clay solutions (Brown et al. 1999; Clarke et al. 1996; Melton and Rand 1977; Mourchid et al. 1995a, 1995b; Ramsay 1986; Rand and Melton 1977). In recent years, organic-inorganic nano-composite materials, which frequently exhibit synergistic behavior and hybrid properties derived from the two components, have attracted the interest of a number of researchers. The large aspect ratio of clay platelets may lead to a supramolecular organization similar to other mesoscopic systems such as liquid crystalline polymers, surfactants, or block copolymers (Kawasumi et al. 1999). Clays find numerous applications in many diverse industrial processes such as coatings in the paper industry, drilling fluids, paints, and ceramic additives, as well as in cosmetic and pharmaceutical formulations (Van Olphen 1977; Weaver and Pollard 1973).

Since shear can influence both the macroscopic texture and the orientation of the underlying anisotropic species, it is helpful to combine different techniques in order to correlate changes in viscoelastic properties with

structural changes on different length scales. Online scattering studies of flowing systems provide insight into the real time state of matter (Fuller 1995; Janeschitz-Kriegl 1983). Industrial processes involve non-equilibrium as well as equilibrium states in the process ranging from preparation to end product application. Therefore real time investigations of this sort are extremely relevant in processing applications. Experimental rheophysical techniques such as small-angle light (SALS) and neutron scattering (SANS), birefringence and dichroism, microscopy, and nuclear magnetic resonance, have been developed to monitor shear-induced structural changes (Fuller 1995; Janeschitz-Kriegl 1983; Nakatani and Dadmun 1995; Sondergaard and Lyngaae-Jorgensen 1995).

Previous investigations on clay solutions proposed many structural models to explain the mesoscopic properties (Fripiat et al. 1982; Lockhart 1980; Morvan et al. 1994; Ramsay and Lindner 1993; Rosta and Von Gunten 1990; Van Olphen 1977) and shear behavior of aqueous clay solutions (Hanley et al. 1994; Mourchid et al. 1995a, 1995b; Pignon et al. 1998). Gelation effects have been described by van Olphen (Van Olphen 1977) by an electrostatic attraction between the positively charged edges and negatively charged faces of the platelets, which results in a linked structure similar to a house of cards. An alternative structure suggested by Norrish et al. explains the gel formation by a long-range electrostatic repulsion between interacting double layers (Norrish 1954).

Rheological studies by Rand and Melton (Melton and Rand 1977; Rand and Melton 1977) on gels formed by Kaolinite dispersions were interpreted in terms of edge-face, edge-edge, and face-face aggregated structures. In contrast, for montmorillonite solutions Rand et al. (1980) found no evidence for edge-face interactions from rheological measurements. Laponite is similar to montmorillonite, a three-layer hectorite type clay with magnesium ions in between the two silicate layers. However the smaller diameter of laponite results in a smaller aspect ratio (30:1) than for montmorillonite (100:1). Under appropriate conditions laponite and montmorillonite platelets may completely exfoliate in aqueous solutions. Saunders et al. (1999), Gabriel et al. (1996), Mourchid et al. (1998), and Ramsay (1986) found evidence for aligned, ordered structures in laponite gels from birefringence and X-ray studies. All these studies were done on quiescent samples. The textures of these birefringent clay gels as observed with polarizing microscopy are typical of a nematic phase. These results were interpreted in terms of repulsive electrostatic interactions. According to Mourchid et al. (1995a, 1995b), laponite particles at the sol-gel transition interact and are not totally free to move separately. One possible way to minimize the total Gibbs energy is to align neighboring particles in order to save free volume and reduce their excluded volume interactions (Mourchid et al. 1995a, 1995b).

A large body of literature exists on the flow behavior of clay solutions (Pignon et al. 1997; Ramsay and Lindner 1993) as well as polymer solutions (Nakatani and Dadmun 1995). However little is known about the influence of shear on viscoelastic clay-polymer solutions (Rossi et al. 1997).

Our previous work described the steady state behavior of a transient polymer-clay network by flow birefringence and SANS of one representative solution of synthetic laponite and poly(ethylene-oxide) (PEO) (Schmidt et al. 2000). With increasing steady shear rate, a pronounced minimum in birefringence was observed corresponding to the orientation of platelets in the flow field followed by an increase in birefringence due to the stretching of polymer chains adsorbed between clay particles at even higher shear rates. In-situ shear-SANS measurements corroborate the shear-induced orientation of the polymer chains and platelets. With increasing shear rate an anisotropic scattering pattern developed. By comparison of the scattering from non-contrast matched samples with contrast matched samples (to the clay), the particles orient before the polymer chains start to stretch and orient (Schmidt et al. 2000). The objective of this contribution is to use rheology and flow birefringence to investigate the synergistic behavior of the same viscoelastic polymer-clay solutions for several different concentrations and to verify the model elucidated from a previous SANS study (Schmidt et al. 2000).

Experimental

The synthetic hectorite type clay, laponite (LRD), was provided by Laporte Industries Ltd. and poly(ethylene-oxide) with a $M_w = 10^6$ g/mol was purchased from Polysciences Inc. The clay particles are composed of platelets of high purity and uniform crystallite size (Pignon et al. 1997; Ramsay et al. 1990). In an aqueous medium, the clay forms transparent dispersions of disk shaped particles ca. 300 Å in diameter and ca. 10 Å thick (Pignon et al. 1997; Ramsay et al. 1990). Various solutions were prepared with a fixed concentration of Laponite at 3 mass % (3% mass fraction) and PEO concentrations ranging from 0 to 5 mass % in distilled, deionized water (Table 1). The samples were mixed for

Table 1 Composition of samples

Sample	PEO mass % (mass fraction)	LRD mass % (mass fraction)
PEO	3	0
LRD	0	3
LRD1	1	3
LRD2	2	3
LRD3	3	3
LRD4	4	3
LRD5	5	3

Relative mass error: $< 1\%$

several minutes a day over at least two weeks. The pH and ionic strength of the solutions were controlled by the addition of NaOH and NaCl, respectively. For all samples in this study a pH value of 10 and a NaCl concentration of 10^{-3} mol/l were used. Under these conditions a flocculation is avoided by balancing van der Waals attraction and electrostatic repulsion of the clay particles (Melton and Rand 1977; Rand and Melton 1977).

Depending on parameters such as pH, the LRD and PEO concentrations, and the ionic strength, different mechanical behavior in polymer-clay solutions can be generated: liquid-like behavior, gel-like phases, rubber-like soft networks, or phase separated liquid and solid phases. The composition window for preparing samples, which behave like soft networks, is very small. A mixture of 3% LRD and 0.1% PEO or less consists of two phases, a water rich phase and polymer-clay rich phases. These phases can be easily separated by centrifuging the samples. The ratio of the water-phase to the solid-like gel-phase is temperature dependent and sensitive to changes in salt concentration and pH. While some samples cannot be mixed homogeneously, LRD1 to LRD5 (Table 1) are one-phase solutions. Prior to shear, all samples are transparent and isotropic. The solutions have network character and during network formation imperfections in the structure may develop. These non-equilibrium structures can be avoided and a homogeneous distribution can be achieved by shearing the samples. The results reported here were obtained on solutions containing the same mass fraction of LRD (3%) and 1–5% PEO at room temperature (Table 1).

Flow birefringence experiments were performed at ambient temperature (≈25 °C) on a Rheometric Scientific, SR 5000 rheometer with an integrated rheo-optical module. The rheometer is equipped with 3.8 cm diameter quartz parallel plate geometry and has a home built solvent trap which allows "evaporation free" experiments for durations up to 7000 s. All rheo-optical experiments, except stress relaxation described later, were performed with the Rheometric SR 5000 instrument within 7000 s. For experiments discussed in this paper, a quartz parallel plate geometry with a gap of 1 mm was used. Additional rheological tests performed with cone and plate geometry produced identical results as parallel plate geometry.

The incident laser beam of the rheo-optical module is parallel to the direction of the velocity gradient. For anisotropic particles, the birefringence is defined as $\Delta n = n_1 - n_2$ assuming orthogonal axes for the refractive indices n_1 and n_2. When elongated particles are exposed to a shear field, they will usually be aligned with their long axes parallel to the flow direction. The orientation of the particles leads to an alignment of the refractive indices n_1 and n_2 where n_1 is always set to be parallel to the flow direction. If the polarizability along the molecular axis is larger along the direction of flow than perpendicular to it, the resulting value of Δn is positive. It is useful to define the retardation, δ, when the birefringence is detected by means of different velocities of the light along the two axes. The retardation is the phase difference of both beams after passing through a material of the thickness, d, and is defined by the equation

$$\delta = 2\pi(\Delta n\ d/\lambda) \tag{1}$$

where λ is the wavelength of the light passing through the sample and d is the path length. Many polymeric liquids show a very simple proportionality between the stress tensor and the refractive index tensor known as the stress optical rule (Janeschitz-Kriegl 1983). Polymer melts, solutions, and many surfactant systems have been shown to conform to the stress optical rule. Our rheometer is equipped with parallel plate geometry with the laser beam parallel to the direction of the velocity gradient (Δn_{13}, 1 is the flow direction, 3 is the vorticity direction). Because of our instrument geometry we can calculate only the Δn_{13} component but not the shear component of the refractive index tensor (Δn_{12}) (Fuller 1995). The interpretation of birefringence is complicated because birefringence can have two different origins. Intrinsic birefringence is due to the optical anisotropy of individual stretched molecules. Form birefringence is due to the difference in the refractive index of the anisotropic particles as compared to their surroundings. It is difficult to estimate a priori whether form or intrinsic birefringence dominates in the case of polymer-clay solutions. In our case the contribution to birefringence from the clay particles can be negative, according to the literature (Fuller 1995; Shah et al. 1963; Yamaoka et al. 1994) and as demonstrated in our experiments on aqueous clay solutions (Schmidt et al. 2000). Also the orientation of the disc normal was determined earlier from shear SANS experiments to be along the vorticity direction (Schmidt et al. 2000).

Stress relaxation experiments described later were performed on a Rheometric Scientific ARES instrument. Since this rheometer had no solvent trap, solvent evaporation had to be taken into account after ca. 3000 s. Data that have been affected by solvent evaporation are suppressed.

Results

In the following, results from mainly LRD2 will be discussed since this sample shows representative properties. Four series of measurements were performed in order to determine the shear orientation of the polymer clay samples: constant shear rate, constant stress (creep experiments), oscillatory shear, and stress relaxation. Constant shear rate and constant stress (creep experiments) will be used to characterize the transient network under steady flow conditions and constant stress (creep experiments), oscillatory shear, and stress relaxation will characterize the elastic network.

Constant rate experiments

The steady shear rate dependence of the viscosity and birefringence was obtained by performing individual, time dependent, constant rate experiments. After cessation of shear the sample was allowed to equilibrate, then another time-dependent, constant rate experiment was performed. Constant shear rates were applied sequentially for ca. 4000 s at low shear rates ($d\gamma/dt < 5\ s^{-1}$) and ca. 1000 s at higher shear rates ($d\gamma/dt > 5\ s^{-1}$). These intervals were sufficient to reach a steady state as determined from both the time dependent viscosity and birefringence measurements. The solutions exhibit shear thinning behavior over the entire range of shear rates as shown by a double logarithmic plot of η vs shear rate, $d\gamma/dt$, (Fig. 1a). Power law exponents ($\eta = (d\gamma/dt)^m$) are in the range of: $m = -0.5(\pm 0.03)$ for LRD1, to $m = -0.6$ (± 0.03) for LRD2 and $m = -0.7$ (± 0.03) for LRD5. It is possible to fit two straight lines to LRD5 ($m = 0.7$ and 0.5); however, for LRD2, LRD3, and LRD4, variations to linearity are in between error bars. If there was a strong correlation between η and Δn, a slope over more decades would be desirable to fit two lines.

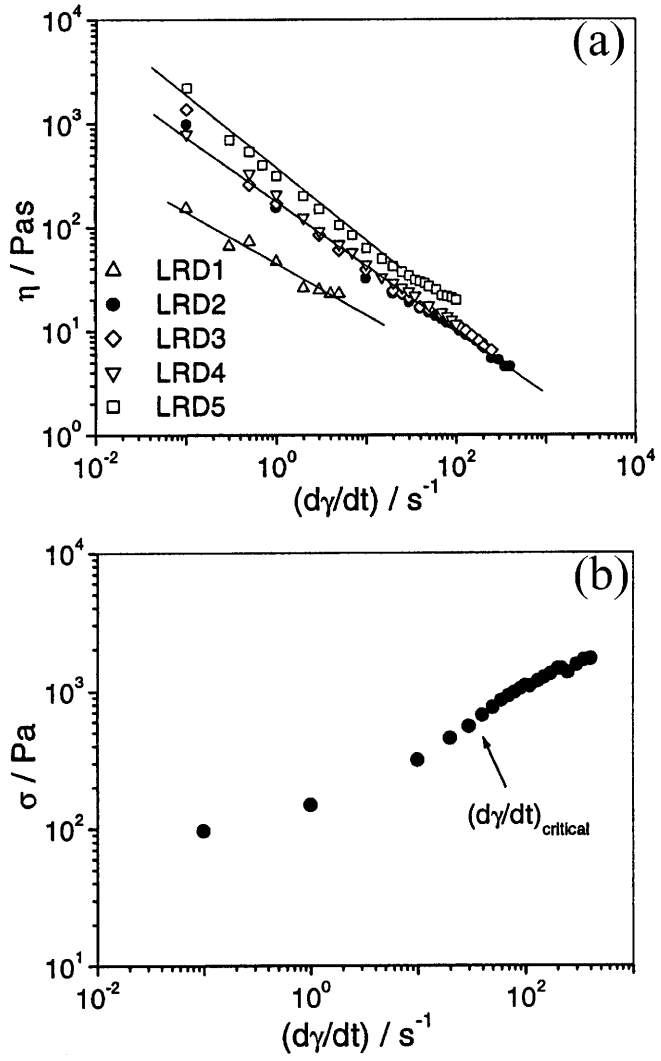

Fig. 1 Steady state values of viscosity as a function of shear rate for LRD1, LRD2, LRD3, and LRD5. The relative standard deviation in the steady state is ca. ±7%. **b** Stress vs shear rate for LRD2. The relative error in the steady state is ca. ±7%

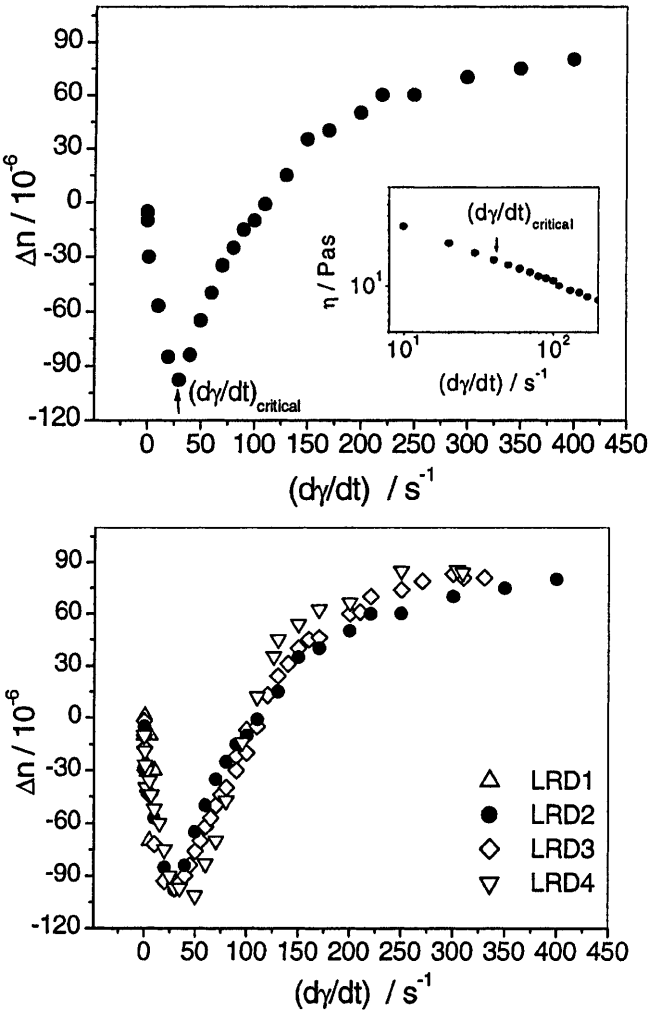

Fig. 2 a Steady state values of birefringence, Δn, as a function of shear rate for LRD2. The relative error in the steady state birefringence is ca. ±4%. *Inlay*: steady state viscosity as a function of shear rates. The relative error on steady state values is approximately ±5%. **b** Steady state values of birefringence, Δn, as a function of shear rate for LRD1 to LRD4. For LRD4 the relative standard deviation in the steady state birefringence is ca. ±9%. LRD1 data are shown for 0.01–20 s^{-1}

The viscosity of LRD1 cannot be measured at shear rates higher than 10 s^{-1} due to wall slip. This effect could be detected when impurity particles in the sample did not move compared to a mark on the quartz plate. More detail of LRD2 may be observed by displaying the stress as a function of shear rate. For LRD2 (Fig. 1b) a slight dip can be observed at shear rates around 50 s^{-1}; however, this dip was in between error bars (≈7%, relative standard deviation) when the experimental series was repeated with a new sample. The steady state values of birefringence as a function of shear rate are shown in Fig. 2. With increasing shear rate we first observe a decrease in birefringence. A distinct minimum in the birefringence is observed at a critical shear rate, $(d\gamma/dt)_{critical}$, of approximately 40 s^{-1} for all concentrations (Fig. 2b). The collection of data is limited at low shear rates by evaporation of solvent during the times necessary to reach steady state. The high shear rates data are limited due to normal forces, which push the sample out of the shear cell. Results from LRD5, not shown here, indicate similar behavior within relative errors of 20%. While the birefringence displays a distinct minimum, the viscosity (Fig. 1a) shows, within a relative error of 5%, no corresponding feature at the critical shear rate. The rate of upturn in birefringence does not change systematically with sample composition.

At low shear rates LRD1 (Table 1) becomes slightly turbid and turns back to clear upon cessation of shear. At

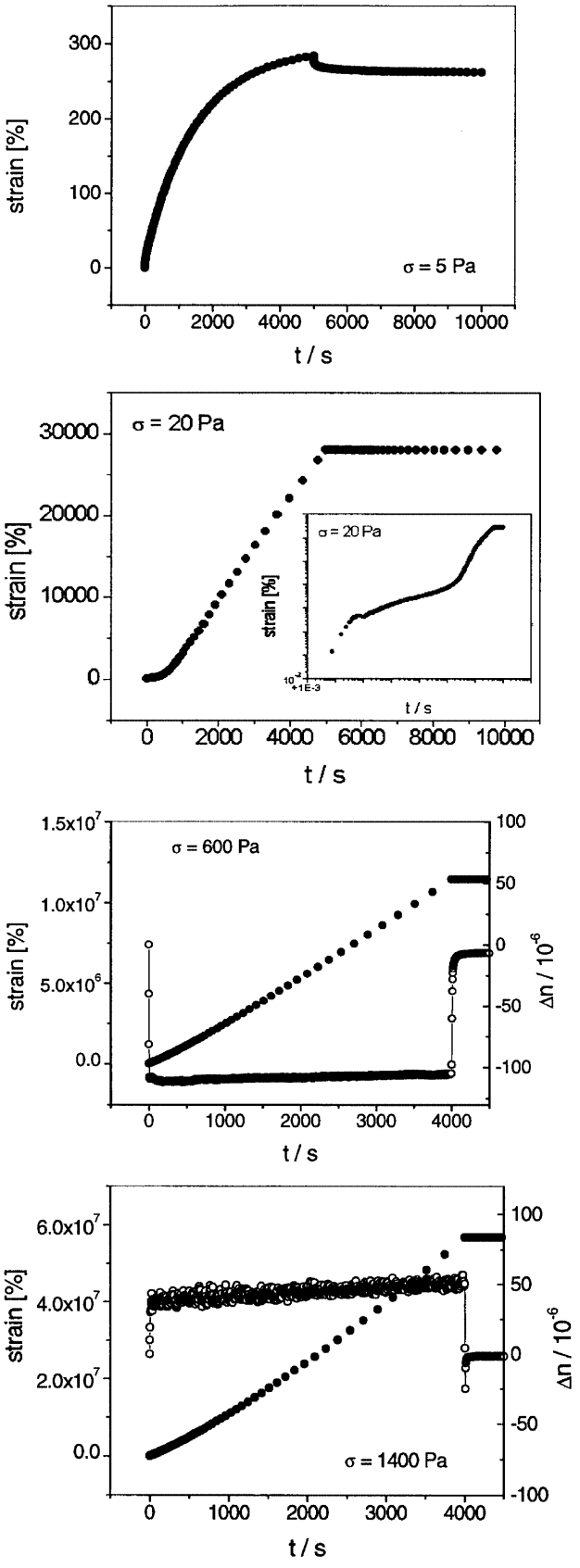

Fig. 3a–d Creep experiments at stresses of: **a** 5 Pa; **b** 20 Pa; **c** 600 Pa; **d** 1400 Pa. *Open circles*: birefringence, *full circles*: strain. Shear was stopped after 5000 s for **a** and **b** and after 4000 s for **c** and **d**

higher shear rates ($>10\ s^{-1}$) we observe slip at the wall sample interfaces. Rheological data as well as flow-birefringence cannot be reproduced for LRD1 at shear rates $>10\ s^{-1}$ under constant rate conditions. At these shear rates ($>10\ s^{-1}$) we observe an aqueous thin film between the shear cell walls and the sample due to shear induced phase separation. This effect is strongly dependent on pH and salt concentration. The remnant film is slightly turbid and elastic. With increasing concentration of PEO, samples in the series LRD2, LRD3, LRD4, LRD5 (see Table 1) become more viscous and adhere to glass.

Constant stress experiments

A series of constant stress (creep) experiments was performed with applied stresses of 1–1400 Pa for LRD2. In Fig. 3 results from several creep experiments are summarized. Figure 3a shows the time dependence and recovery of the strain at 5 Pa. At 20 Pa (Fig. 3b) the sample showed no strain recovery after cessation of shear (= 5000 s). The insert in Fig. 3b shows a logarithmic plot of these data. After ca. 60 s (strain ca. 40–50%) the viscosity decreased, the material started to flow, and no strain recovery was observed. No significant flow-birefringence was observed for both experiments.

For experiments at stresses higher than 50 Pa, a constant shear stress was applied over 4000 s. A "steady state" was characterized by constant viscosity and constant birefringence. Steady state values were independent of shear history. Figure 3c,d shows the time dependence of two measurements in more detail. During the first creep experiment at $\sigma = 600$ Pa steady shear flow was reached within a few minutes and a constant negative Δn plateau was found, indicating a stable flow. During the second creep experiment with $\sigma = 1400$ Pa steady flow was reached after 2000 s and a positive value of Δn was observed. Both creep experiments show that the plateau in Δn is reached in less than 20 s; however in this time steady state viscosity is not reached. The Δn value stayed constant until the shear was stopped. After cessation of shear the sample relaxed to $\Delta n = 0$ in less than 150 s. No strain recovery was observed for experiments at stresses >20 Pa. During creep experiments at stresses >1500 Pa and over a long period of time (≈4 h) the sample structure was destroyed and Δn did not recover after cessation of shear.

Figure 4 shows steady state values of viscosity and corresponding birefringence when a constant stress was applied. With increasing stress we observe (similar to constant rate experiments) a decrease in birefringence. A

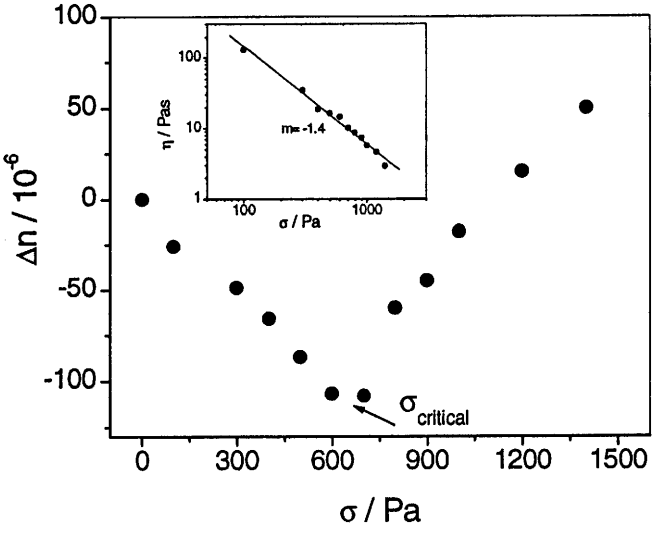

Fig. 4 Steady state values of birefringence, Δn, as a function of stress for LRD2. The relative error in the steady state birefringence is ca. ±4%. *Insert*: steady state viscosity as a function of stress. The relative standard deviation on steady state values is approximately ±5%

distinct minimum in the birefringence is observed at a critical shear stress of approximately 600 Pa for LRD2. While the birefringence displays a minimum, the viscosity and corresponding shear rate show no corresponding feature at the critical shear stress. These data are in agreement with results from constant rate experiments. Strain values ($\gamma(t) = J(t) \cdot \sigma$) (not shown here) as obtained from creep experiments as a function of applied stress σ and time t indicate no significant signature which corresponds to the minimum in birefringence, neither as a function of stress nor time.

Oscillatory shear

Since it is not possible to perform simultaneous dynamic mechanical and birefringence experiments with the Rheometric Scientific SR 5000 instrument, only rheological data will be presented in this section. Frequency dependent oscillatory shear of LRD1 showed a simple behavior. A broad linear viscoelastic range and a frequency independent storage modulus of $G' = 4.5 \times 10^3$ Pa was observed over several decades. The reference sample (LRD) with 3% LRD containing no polymer showed similar behavior (Fig. 5a). The loss modulus was always smaller than G′, and thus the sample behaved as an elastic solid. From an oscillatory stress dependent experiment at 1.5 Hz ($\omega = 2\pi\nu$), however, LRD started to flow when a strain of ca. 12% was exceeded (Fig. 5b).

LRD2 storage and loss moduli are shown in Fig. 6a at a frequency of 1 Hz as a function of stress along with

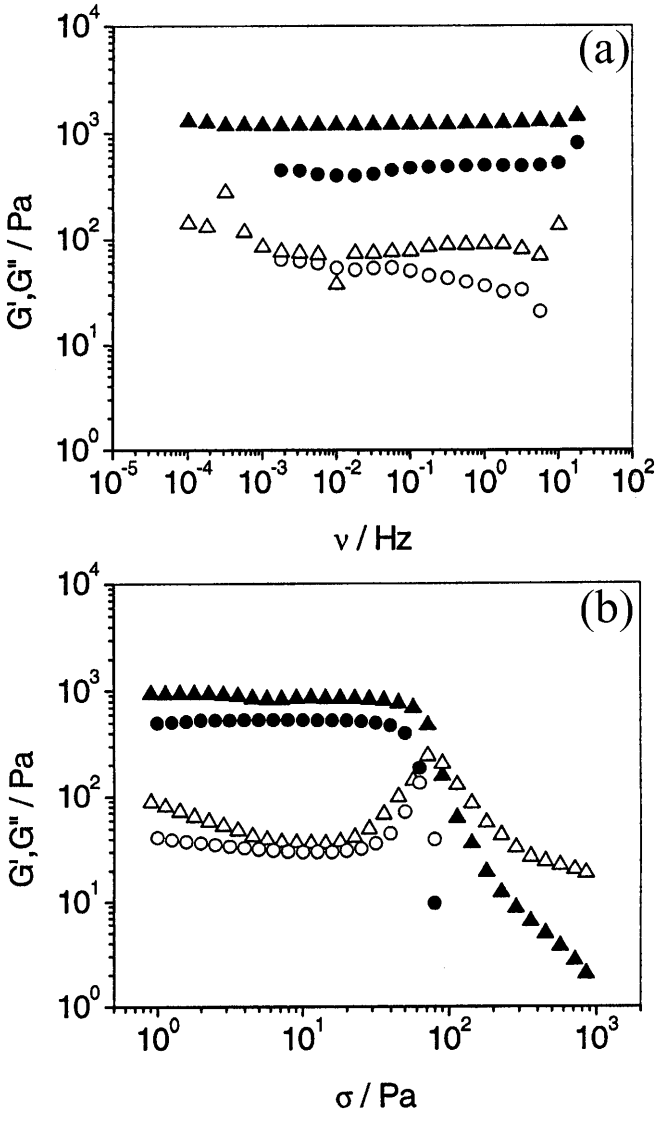

Fig. 5 a Frequency dependence of G′ and G″ for the reference LRD sample (*circle*) and LRD1 (*triangle*) at a shear stress of $\sigma = 5$ Pa. **b** Stress dependence of G′ (*full symbols*) G″ (*open symbols*) for LRD1 and LRD at a frequency of 1.5 Hz. Experiments could be reproduced with a new sample within a relative standard deviation of ≈9%

the strain as a function of stress (Fig. 6b). At low strains up to ca. 30% the sample behaves elastically and above this critical strain the sample started to flow. The same critical strain was observed in stress-controlled as well as strain-controlled dynamic experiments. The critical strain value upon which flow occurred is frequency independent in a range from 0.1 to 10 Hz. While LRD2 started to flow at critical strains of ca. 30%, LRD4 and LRD5 showed this behavior around strains of 50% and 75%.

Frequency dependent experiments (not shown here) indicate viscoelastic behavior (G′ > G″). The flow, however, did not change the equilibrium structure of

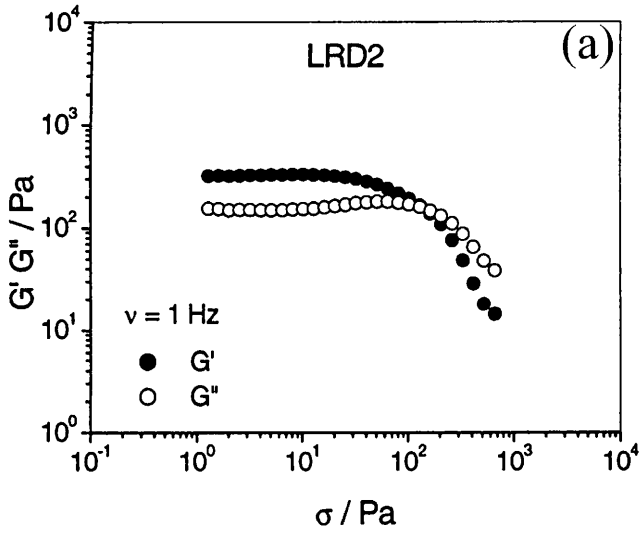

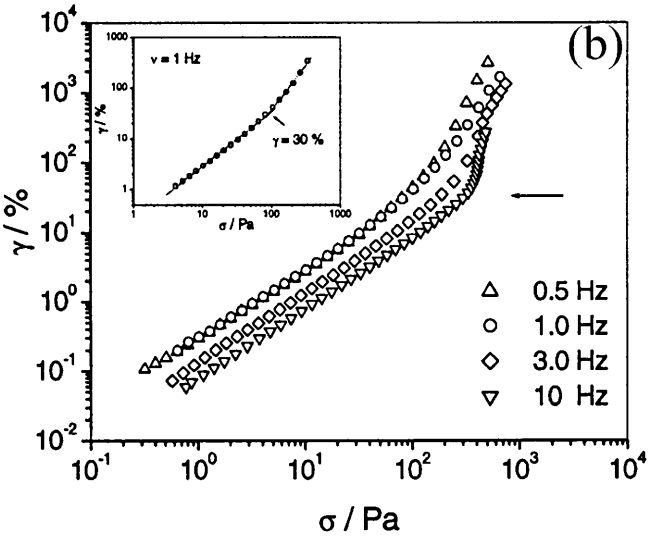

Fig. 6a, b Stress dependence of G′ and G″ for LRD2 at a frequency of: **a** 1 Hz; **b** strains as a function of applied stress. G′ *filled symbols*, G″ *open symbols*. Experiments could be reproduced with a new sample within a relative standard deviation of ≈9%

the samples at rest and all experiments could be reproduced when repeated.

Stress relaxation

Several stress relaxation experiments were performed on LRD2 in order to characterize the response of the polymer-clay network to a step change in strain (Fig. 7). At imposed strains smaller than 30% we observe first a linear response of the relaxation modulus with slopes of $m = -0.17$ (0.5% strain), $m = -0.13$ (1.0% strain), and $m = -0.13$ (10% strain) over the first 200 s (Table 2). During a stress relaxation exper-

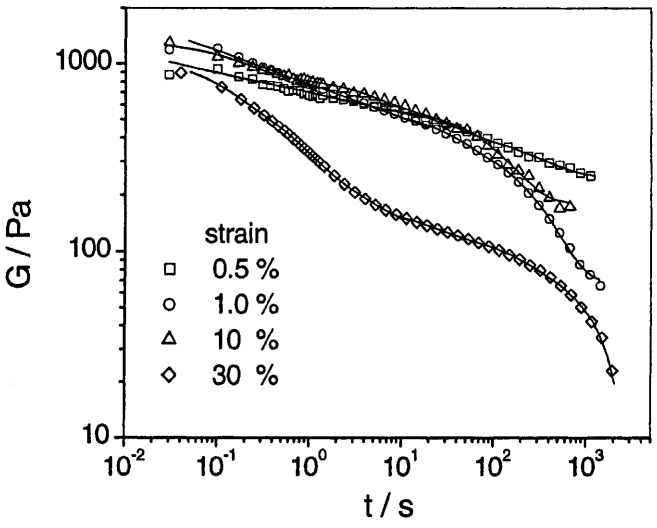

Fig. 7 Stress relaxation experiments at commanded strains of 0.5% (*square*), 1.0% (*circle*), 10% (*triangle*), and 30% (*diamond*). *Solid lines* show corresponding fit curves

iment with an imposed strain of 30% we observe no linear response but several relaxation times. Experimental analyses of stress relaxation data have assumed a series of relaxation times t defined as $G(x) = \sum G_k \cdot \exp(-x/t)$ with G_k the weighting constant (Macosko 1994). For all experiments two significant relaxation times could be detected over ca. 1000 s. With increasing strain, t1 and t2 decrease from 30 to 17 s and 316 to 174 s, respectively (Table 2). A plot of t1 or t2 vs applied strain shows no linear behavior. Experiments covering longer times than ca. 3000 s were not possible due to evaporation of solvent.

Discussion

All polymer-clay solutions discussed in this article contain more than 90% of water and show elastic as well as flow behavior. In our previous work, we proposed that the polymer chains were in dynamic adsorption/desorption equilibrium with the clay platelets to form a network. All polymer-clay samples consist of a network between randomly oriented clay platelets and PEO chains with polymer chains as dynamic crosslinks between the platelets.

The steady state values of viscosity as a function of shear rate show shear thinning over the entire range of shear rates as indicated by a double logarithmic plot of η vs shear rate (Fig. 1). The shear thinning originates from the orientation of clay particles and induced conformational changes of polymer chains due to a continuously created and destroyed network of polymer-clay connections. Under flow conditions polymer chains are in

Table 2 Relaxation times and slopes for stress relaxation experiments described in Fig. 7

Strain/%	Slope	$(t_1/s)^a$	$(t_2/s)^a$
0.5	−0.17	30.1	316.2
1.0	−0.18	30.4	295.0
10	−0.13	28.5	228.7
30	0.1, 0.6, 3.6[b]	17.2	174.1

[a] t_1, t_2: relaxation times
[b] Relaxation times for an imposed strain of 30%
Standard deviation ≈ 10% for t1 and t2 at 10% strain (due to solvent evaporation); standard deviation < 3% for all other relaxation times

cooperative adsorption/desorption equilibrium of a transient network. This is the reason why the power law exponents become more negative with increasing PEO concentration. Figure 1b shows the stress dependence as a function of shear rate for LRD2. A slight dip is observed at shear rates around 50 s^{-1} (Fig. 1b). However, in a range of errors of ca. 7% (relative standard deviation) one cannot determine if this dip is significant.

The birefringence behavior shown in Fig. 2 suggests a "saturated network" is reached at a polymer concentration of ca. 2% PEO and 3% LRD (LRD2). At this concentration all possible cross-links between polymer and clay are created and the surface of the clay platelets is saturated with polymer. Below this concentration no significant birefringence can be observed because a strong network is not yet established and thus cannot be stretched. A small angle neutron scattering study by Lal and Auvray (2000) describes nicely the adsorption of polymer chains to clay platelets at low polymer and clay concentrations. A 2% solution of PEO, at the same pH, polymer, and salt concentration produced no significant birefringence ($\Delta n \approx 2\ (\pm 0.5) \times 10^{-6}$) at shear rates up to 100 s^{-1}. Similarly a 3% aqueous clay solution showed only slight negative birefringence ($\Delta n \approx -12\ \ (\pm 8) \times\ 10^{-6}$). This birefringence is less negative than the minimum birefringence of the clay-polymer solution.

Above concentrations representing LRD2 (Table 1) we observe strong flow-birefringence and no significant change in birefringence with increasing PEO concentration (Fig. 2b). As soon as the network is established the left over PEO remains in solution as either a shear thickener or covers and saturates the clay platelets with polymer. While birefringence displays a distinct minimum, neither viscosity nor corresponding stress (Fig. 1a,b) exhibit a significant signature of critical shear rate showing that birefringence is much more sensitive to orientational effects than rheology. While birefringence detects orientational effects on microscopic length scales, rheology averages over macroscopic changes in the sample.

Birefringence is due to anisotropies of the refractive index in the sample. When the sample is free of stress and the polymer chains and clay platelets are randomly oriented, the total refractive index, n, will be isotropic. With increasing shear rate, we first observed a decrease in birefringence. At $(d\gamma/dt)_{critical}$, the birefringence of the stretched polymer chains starts to affect the total birefringence value. The contribution to birefringence from stretched polymer chains will be positive with chains oriented in the flow direction (Fuller 1995; Janeschitz-Kriegl 1983). Above $(d\gamma/dt)_{critical}$ the orientation of the clay continues to increase as well as the Δn contribution of the stretched polymer, and therefore the total birefringence becomes positive.

If strains in a polymer clay network are small, the chains are not displaced significantly from their equilibrium conformations corresponding to more or less isotropic random coils. This behavior is similar to rubbers or entangled polymers. The clay platelets orient in the shear field, which leads to an anisotropy in the refractive index and therefore the birefringence. A disk-like particle will have three principal symmetry axes and therefore three refractive index components. Two of the axes are equivalent due to the geometry of the platelet. The third symmetry axis is normal to the disk plane. The contribution to birefringence from the clay particles can be negative, according to the literature (Fuller 1995; Shah et al. 1963; Yamaoka et al. 1994) and as demonstrated in our experiments on aqueous clay solutions (Schmidt et al. 2000).

From our negative birefringence data we can determine that the platelets are oriented along the flow direction but we cannot determine the direction of the normal to the disc plane. However, the orientation of the disc normal was determined earlier from shear SANS experiments to be along the vorticity direction (Schmidt et al. 2000). The total birefringence may consist of intrinsic and form birefringence of clay platelets and polymer chains. As shown above, at shear rates up to 30–40 s^{-1}, birefringence is dominated by the orientation of clay. Δn is independent of the PEO concentration (Fig. 2b) and the minimum in birefringence occurs at the same shear rate for all PEO concentrations. Initially with shear there is compensation between the negative components of birefringence of the clay and the positive components of the stretched polymer. At higher shear rates, contributions to Δn with opposite signs compensate to give $\Delta n = 0$ even though increasing alignment. This birefringence behavior is due only to the unique structure of a sheared polymer clay network. At shear rates higher than 400 s^{-1}, the polymer concentration may have influence on the total birefringence. In addition to the polymer to clay connections there are still entanglements between polymer chains possible and interactions to excess PEO molecules that are not connected to the clay. However it seems reasonable that

positive birefringence comes from the stretched polymer chains due to polymer-clay interactions and not from the excess PEO concentration in the sample, since Δn is not significantly dependent on the PEO concentration (Fig. 2b). Additional PEO molecules inside the network act only as shear thickener. The recovery of birefringence is much faster than expected from Brownian motion and indicates high elasticity.

Steady state flow behavior was characterized by creep and constant rate experiments. Both experimental methods reveal similar behavior under steady state viscosity conditions. Each steady state is characterized by constant viscosity and birefringence and can be reached by applying either a constant stress or a constant shear rate. Figure 4 shows a distinct minimum in birefringence at ca. 600 Pa. This value corresponds to a shear rate of ca. 40 s^{-1}, which is the critical shear rate from constant rate experiments. As expected from constant rate experiments, we observe that viscosity, shear rate, and strain show no significant signature of critical stress.

Oscillatory shear and stress relaxation experiments of LRD2 show essentially the elastic response at small strains and a typical network character. At strains up to 30%, LRD2 samples behave elastically and above a critical strain of ca. 30% the network structure is being disrupted and the sample started to flow. For LRD4 and LRD5 this point is reached at a critical strain of 50% and 75% suggesting an influence of PEO concentration on the network strength. Our current understanding is that the polymer chains are in dynamic adsorption/desorption equilibrium with the clay particles to form a network. At a strain of 30% (LRD2) flow starts and kinetics of this adsorption/desorption equilibrium starts to change. At this point the sample undergoes a transition from a transient network to a dynamic network with strong strain dependent adsorption/desorption kinetics. Although one would expect a gel like behavior with a stress dependency of flow, the observed behavior is similar to a polymer melt resembling a transient network of entangled polymers. At low strains the network is not disturbed significantly and the samples behave as elastic solids. The elastic part in the response of the polymer-clay system is due to the transient network character. With increasing strain, tension in PEO strand builds up along the lines of flow, chains are extended on stretching the network and kinetics of the adsorption/desorption process become faster. As the tension of polymer strand between clay particles increases with the strain (critical strain), the kinetics of the desorption/adsorption equilibrium change and the chains recoil, rearrange, and reconnect. This is the point where strong flow starts in oscillatory shear experiments and a steady state is detected under steady shear. At very high shear rates (>400 s^{-1}) desorption becomes faster than the adsorption process, density fluctuations are generated, and the sample structure is being destroyed.

A series of stress relaxation experiments on LRD2 characterizes the response of the polymer-clay network to a step change in strain (Fig. 7). At imposed strains smaller than 30% we observe first a linear response of the relaxation modulus over the first 100 s (Table 2). Here the relaxation behavior is due to a dominant elastic response of the network (transient network). For all experiments two significant relaxation times could be detected over ca. 1000 s. Relaxation times originate from the clay, the polymer-clay, or the polymer itself. During a stress relaxation experiment with an imposed strain of 30% we observe no linear response but several relaxation times. At this strain the sample relaxes from a state of flow to a state of full recoverability of the network structure. Relaxation times observed in this experiment can be attributed to the relaxation of the polymer, the relaxation of the clay, and a relaxation due to polymer-clay interactions since the sample relaxes from a dynamic network with dominating viscous properties to an elastic network at rest. At this point relaxation times cannot be decoupled. Future work will compare results from rheology with dynamic light scattering data and will correlate the corresponding relaxation times with the normal modes in the polymer-clay system.

Conclusion

The shear orientation of viscoelastic clay-polymer solutions was investigated by means of rheology and flow birefringence (Δn). The polymer chains are in dynamic adsorption/desorption equilibrium with the clay particles to form a ''network''. The elastic behavior of the network was characterized by constant stress, oscillatory shear, and stress relaxation experiments. Experiments under steady flow characterized the transient behavior of the network. With increasing steady shear rate a pronounced minimum in birefringence is observed, showing that clay platelets orient first, and at a critical shear rate polymer chains start to stretch. The shear rate dependent viscosity showed near power law behavior and no corresponding critical feature. While birefringence detects orientational effects on a microscopic length scale, rheology averages over macroscopic changes in the sample.

Acknowledgements Financial support by the Alexander von Humboldt Foundation is gratefully acknowledged by Gudrun Schmidt. We thank Dr. Carl Schultheisz for fruitful discussions and the reviewers for useful suggestions and comments.

References

Bates FS, Koppi KA, Tirrell M, Almdal K, Mortensen K (1994) Influence of shear on the hexagonal to disorder transition in a diblock copolymer melt. Macromolecules 27:5934–5936

Brown ABD, Ferrero C, Narayanan T (1999) Phase separation and structure in a concentrated colloidal dispersion of uniform plates. Eur Phys J B 11(3): 481–489

Clarke SM, Rennie AR, Convert P (1996) A diffraction technique to investigate the orientational alignment of anisotropic particles: studies of clay under flow. Europhys Lett 35(3):233–238

Fripiat J, Cases J, Francois M, Letellier M (1982) Thermodynamic and microdynamic behavior of water in clay suspensions and gels. J Colloid Interface Sci 89(2):378–400

Fuller GG (1995) Optical rheometry of complex fluids. Oxford-University-Press, Oxford

Gabriel JCP, Sanchez C, Davidson P (1996) Observation of nematic liquid-crystal textures in aqueous gels of smectite clays. J Phys Chem 100(26):11,139–11,143

Hanley HJM, Straty GC, Tsvetkov F (1994) A small-angle neutron-scattering study of a clay suspension under shear. Langmuir 10(9):3362–3364

Jamieson AM, Gu DF, Chen FL, Smith S (1996) Viscoelastic behavior of nematic monodomains containing liquid crystal polymers. Prog Polym Sci 21(5):981–1033

Janeschitz-Kriegl H (1983) Polymer melt rheology and flow birefringence. Springer, Berlin Heidelberg New York

Kawasumi M, Hasegawa N, Usuki A, Okada A (1999) Liquid crystal/clay mineral composites. Appl Clay Sci 15(1/2):93–108

Lal J, Auvray L (2000) Interaction of polymer with clay. J Appl Cryst 33:673–676

Lockhart NC (1980) Electrical properties and the surface characteristics and structure of clays. 1. Swelling clays. Colloid Interface Sci 74(2):509–519

Macosko CW (1994) Rheology, principles, measurements and applications. Wiley-VCH, New York Chichester Weinheim Brisbane Singapore Toronto

Melton IE, Rand B (1977) Particle interactions in aqueous kaolinite suspensions. 2. Comparison of some laboratory and commercial kaolinite samples. J Colloid Interface Sci 60(2):321–330

Morvan M, Espinat D, Lambard J, Zemb T (1994) Ultrasmall-angle and small-angle X-ray-scattering of smectite clay suspensions. Colloids Surf 82(2): 193–203

Mourchid A, Delville A, Levitz P (1995a) Sol-gel transition of colloidal suspensions of anisotropic particles of laponite. Faraday Discuss 101:275–285

Mourchid A, Delville A, Lambard J, Lecolier E, Levitz P (1995b) Phase-diagram of colloidal dispersions of anisotropic charged-particle-equilibrium properties, structure, and rheology of laponite suspensions. Langmuir 11(96):1942–1950

Mourchid A, Lecolier E, Van Damme H, Levitz P (1998) On viscoelastic, birefringent, and swelling properties of laponite clay suspensions: revisited phase diagram. Langmuir 14(17): 4718–4723

Nakatani AI, Dadmun MD (1995) Flow-induced structure in polymers. ACS, Washington

Nakatani AI, Morrison FA, Jackson CL, Douglas JF, Mays JW, Muthukumar M, Han CC (1996) Shear-induced changes in the order-disorder transition temperature and the morphology of a triblock copolymer. J Macromol Sci Phys B35(3/4):489–503

Norrish K (1954) The swelling of montmorillonite. Discuss Faraday Soc 120–134

Pignon F, Magnin A, Piau JM, Cabane B, Lindner P, Diat O (1997) Yield stress thixotropic clay suspension: investigation of structure by light, neutron, and X-ray scattering. Phys Rev E 56:3281–3289

Pignon F, Magnin A, Piau JM (1998) Thixotropic behavior of clay suspensions: combinations of scattering and rheometric techniques. J Rheol 42(6): 1349–1373

Ramsay JDF (1986) Colloidal properties of synthetic hectorite clay dispersions. 1. Rheology. J Colloid Interface Sci 109(20):441–447

Ramsay JDF, Lindner P (1993) Small-angle neutron scattering investigations of the structure of thixotropic dispersions of smectite clay colloids. J Chem Soc Faraday Trans 89(23):4207–4214

Ramsay JDF, Swanton SW, Bunce J (1990) Swelling and dispersions of smectite clay colloids – determination of structure by neutron-diffraction and small-angle-neutron scattering. J Chem Soc Faraday Trans 86(23):3919–3926

Rand B, Melton IE (1977) Particle interactions in aqueous kaolinite suspensions. 1. Effect of pH and electrolyte upon mode of particle interaction in homoionic sodium kaolinite suspensions. J Colloid Interface Sci 60(2):308–320

Rand B, Pekenc E, Goodwin JW, Smith RW (1980) Investigation into the existence of edge-face coagulated structures in Na-montmorillonite suspensions. J Chem Soc Faraday Trans 1 76:225–235

Rossi S, Luckham PF, Zhu S, Briscoe BJ, Tadros TF (1997) Influence of low molecular weight polymers on the rheology of bentonite suspensions. Rev Inst Fr Pet 52(2):199–206

Rosta L, von Gunten HR (1990) Light-scattering characterization of laponite sols. J Colloid Interface Sci 134(2):397–406

Roux D, Nallet F, Diat O (1993) Rheology of lyotropic lamellar phases. Europhys Lett 24(1):53–58

Saunders JM, Goodwin JW, Richardson RM, Vincent B (1999) J Phys Chem B 103(43):9211–9218

Schmidt G, Richtering W, Lindner P, Alexandridis P (1998) Shear-orientation of a hexagonal lyotropic triblock copolymer phase as probed by flow birefringence and small-angle light and neutron scattering. Macromolecules 31(7):2293–2298

Schmidt G, Nakatani AI, Butler PD, Karim A, Han CC (2000) Shear orientation of viscoelastic polymer-clay solutions probed by flow birefringence and SANS. Macromolecules 33(20): 7219–7222

Shah M, Thomson DC, Hart CM (1963) Reversal of electro-optical birefringence in bentonite suspensions. J Phys Chem 67:1170–1178

Sondergaard K, Lyngaae-Jorgensen J (1995) Rheo-physics of multiphase polymer systems. Technomic, Lancaster, Pennsylvania, Basel, Switzerland

Van Olphen H (1977) An introduction to clay colloid chemistry. Wiley-Interscience, New York

Weaver CE, Pollard LD (1973) The chemistry of clay minerals. Elsevier, Amsterdam

Yamaoka K, Sasai R, Ikuta N (1994) Reversing-pulse birefringence of montmorillonite particles suspended in aqueous media. Chem Lett 563–566